

Research Paper

Effective targeted therapy for drug-resistant infection by ICAM-1 antibody-conjugated TPGS modified β -Ga₂O₃:Cr³⁺ nanoparticles

Xu-Qi Kang¹, Gao-Feng Shu¹, Sai-Ping Jiang², Xiao-Lin Xu¹, Jing Qi¹, Fei-Yang Jin¹, Di Liu¹, Yong-Hong Xiao³, Xiao-Yang Lu^{2,✉}, Yong-Zhong Du^{1,✉}

1. College of Pharmaceutical Sciences, Zhejiang University, 866 Yuhangtang Road, Hangzhou 310058, China.
2. Department of pharmacy, The First Affiliated Hospital, College of Medicine, Zhejiang University, Hangzhou, 310006, China.
3. State Key Laboratory for Diagnosis and Treatment of Infectious Diseases, Collaborative Innovation Center for Diagnosis and Treatment of Infectious Diseases, The First Affiliated Hospital, College of Medicine, Zhejiang University, Hangzhou, 310006, China.

✉ Corresponding authors: duyongzhong@zju.edu.cn (Yong-Zhong Du); xiaoyanglu@zju.edu.cn (Xiao-Yang Lu).

© Ivyspring International Publisher. This is an open access article distributed under the terms of the Creative Commons Attribution (CC BY-NC) license (<https://creativecommons.org/licenses/by-nc/4.0/>). See <http://ivyspring.com/terms> for full terms and conditions.

Received: 2019.01.23; Accepted: 2019.03.18; Published: 2019.04.13

Abstract

The prevalence of antibiotic resistance and lack of alternative drugs have posed an increasing threat to public health. Here, we prepared β -Ga₂O₃:Cr³⁺ nanoparticles modified with ICAM1-antibody-conjugated TPGS (I-TPGS/Ga₂O₃) as a novel antibiotic carrier for the treatment of drug-resistant infections.

Methods: I-TPGS/Ga₂O₃ were firstly characterized by measuring particle size, morphology, crystal structure, drug loading capacity, and *in vitro* drug release behaviors. The *in vitro* antibacterial activities of I-TPGS/Ga₂O₃/TIG were evaluated using standard and drug-resistant bacteria. The internalization of I-TPGS/Ga₂O₃ was observed by fluorescence confocal imaging, and the expression levels of the efflux pump genes of TRKP were analyzed by real-time RT-PCR. *In vitro* cellular uptake and *in vivo* biodistribution study were performed to investigate the targeting specificity of I-TPGS/Ga₂O₃ using HUEVC and acute pneumonia mice, respectively. The *in vivo* anti-infective efficacy and biosafety of I-TPGS/Ga₂O₃/TIG were finally evaluated using acute pneumonia mice.

Results: It was found that TPGS could down-regulate the over-expression of the efflux pump genes, thus decreasing the efflux pump activity of bacteria. I-TPGS/Ga₂O₃ with small particle size and uniform distribution facilitated their internalization in bacteria, and the TPGS modification resulted in a significant reduction in the efflux of loaded antibiotics. These properties rendered the encapsulated tigecycline to exert a stronger antibacterial activity both *in vitro* and *in vivo*. Additionally, targeted delivery of I-TPGS/Ga₂O₃ mediated by ICAM1 antibodies contributed to a safe and effective therapy.

Conclusion: It is of great value to apply I-TPGS/Ga₂O₃ as a novel and effective antibiotic delivery system for the treatment of drug-resistant infections.

Key words: β -Ga₂O₃:Cr³⁺; Tocopherol polyethylene glycol succinate; Drug-resistance bacteria; Targeted antibiotic delivery; Bioimaging

Introduction

Klebsiella pneumoniae (KPN) has emerged as one of the major nosocomial pathogens threatening the public health worldwide, since it could cause multiple infections in patients with low immunity, including

pneumonia, liver abscess, urinary tract infection, meningitis, and bacteremia [1]. Furthermore, the easy access to multiple drug resistance and strong dissemination ability make KPN seriously threaten

the human health [2, 3]. Recently, the increasingly acquisition of severe resistance to antibiotics and scarcity of effective treatments have aroused public concern and awareness of these great difficulties and challenges brought to clinical treatment [1].

There are limited alternative drugs for multi-drug resistant KPN infection, among which tigecycline (TIG) is one of the remained most active antibacterial agents worldwide [4]. However, with the increase of clinical application, the steady increased drug resistance rate and decreased sensitivity to TIG have threatened these last line therapies [5]. Therefore, it is of great research value and clinical significance to find effective means to overcome the resistance of KPN to TIG. Pulmonary infection caused by multidrug-resistant KPN is one of the most common infections [6]. Due to the lack of available alternative drugs, TIG is commonly used "off-label" for "off label" indications (78%) in nosocomial pneumonia with multidrug-resistant KPN infection [7]. Moreover, in clinical treatment, it is often necessary to increase the dose of TIG to increase the concentration of drug in the lung. The increased dosage of TIG is usually accompanied with an increase in serious adverse reactions, thereby resulting in a clinical treatment failure. Therefore, how to increase the concentration of drug in the lung and reduce the systemic adverse reactions has become another urgent problem in TIG application.

Nano-drug delivery system (DDS) has been extensively used in tumor targeting therapy and drug resistance [8-10]. In addition, previous studies have suggested that some nanocarrier systems could improve the efficacy of antibacterial drugs and reduce the adverse reactions by improving the biodistribution and permeability of drugs to the target tissues and avoiding nonspecific diffusion to normal organs [11-14]. In the meantime, in order to achieve personalized diagnose and treatment, it is necessary to monitor the biodistribution of DDS *in vivo*. Thus, multi-functional nanoparticles for bioimaging and drug loading can come in handy. As a wide-band gap semiconductor material, β -Ga₂O₃:Cr³⁺ have attracted wide attention due to their special conductivity and luminescent properties. By doping with different rare earth or transition metal elements, β -Ga₂O₃ can radiate various photoluminescence spectra from visible light to near-infrared light [15-17]. Although β -Ga₂O₃:Cr³⁺ has been widely used in optoelectronic devices, there are very few studies on the simultaneous application of gallium oxide for *in vivo* imaging and drug delivery.

Furthermore, in order to combat the bacterial resistance and achieve targeted therapy, surface modification of the nanoparticles is needed.

Polyethylene glycol vitamin E succinate (TPGS) is considered as a safe and excellent nonionic surfactant, which is widely used in DDS. Recent studies have revealed that TPGS can reduce the resistance of multidrug-resistant tumor cells by inhibiting the efflux function of efflux pumps [18, 19]. The mechanism of drug resistance in tigecycline-resistant *Klebsiella pneumoniae* (TRKP) is related to the high expression of RND-type efflux pump genes (AcrAB and OqxAB) and upstream binding site (ramA) [20-22]. Therefore, the application of TPGS to inhibit the expression of bacterial efflux pump genes may be an innovative and effective approach to combat TRKP and treat pneumonia caused by TRKP infection. On the other hand, by modifying the surface of nanocarriers with ICAM1 antibody, targeted delivery of endothelial cells and inflammatory sites could be achieved through the specific binding of ICAM1 antibody to ICAM1 receptor on the surface of endothelial cells [23-25]. The expression of ICAM1 in KPN infected mice was significantly up-regulated [26], suggesting that DDS modified with ICAM1 antibody is expected to achieve targeted drug delivery in the treatment of TRKP pulmonary infection.

Here, we firstly prepared β -Ga₂O₃:Cr³⁺ nanoparticles for loading the antibacterial drug of TIG. To achieve targeting capabilities and bacterial resistance inhibition, the TIG-loaded β -Ga₂O₃:Cr³⁺ nanoparticles were subsequently modified with ICAM-1 antibody-conjugated TPGS. The morphology characteristics, *in vitro* bacterial internalization, drug resistance inhibition, cellular uptake and lung targeting ability of anti-ICAM1-TPGS/ β -Ga₂O₃:Cr³⁺ were investigated in detail. *In vitro* and *in vivo* antibacterial activities of anti-ICAM1-TPGS/ β -Ga₂O₃:Cr³⁺/TIG were further studied.

Results and Discussion

Preparation and characterization of β -Ga₂O₃:Cr³⁺ nanoparticles

Firstly, the GaOOH:Cr³⁺ nanoparticle as a precursor was prepared at a mild temperature of 95 °C (atmospheric pressure) via the adjustment of pH of different reaction mediums. The preparation of β -Ga₂O₃:Cr³⁺ nanoparticles were improved by the method described in our previous research [17]. First, the precursor GaOOH:Cr³⁺ nanoparticles were synthesized via hydrothermal method. However, unlike most other hydrothermal processes used to synthesize GaOOH:Cr³⁺ (>200 °C and reaction kettle) [27, 28] we managed to achieve the synthesis of GaOOH:Cr³⁺ under milder reaction conditions by adjusting the reaction medium, pH and temperature (95 °C, atmospheric pressure). In addition to greater

safety and ease of operation, this modified hydrothermal method also helps to expand the reaction capacity. The transmission electron microscopy (TEM) images revealed that the $\text{GaOOH}:\text{Cr}^{3+}$ nanoparticles prepared by the hydrothermal method was spindle-shaped, and evenly distributed with particle sizes of 10-20 nm (Figures 1A&B). Then, the $\beta\text{-Ga}_2\text{O}_3:\text{Cr}^{3+}$ nanoparticles were obtained by high temperature calcination of $\text{GaOOH}:\text{Cr}^{3+}$. We found that the $\beta\text{-Ga}_2\text{O}_3:\text{Cr}^{3+}$ nanoparticles had particle size distributions of around 15 nm, but they were severely aggregated when they were dispersed in water (Figures 1A&B). On the other hand, the $\beta\text{-Ga}_2\text{O}_3:\text{Cr}^{3+}$ nanoparticles showed well-dispersivity in water with slight change in the sizes when TPGS was added into the system. This result

suggested that TPGS as a surfactant was successfully adsorbed onto the surfaces of $\beta\text{-Ga}_2\text{O}_3:\text{Cr}^{3+}$ nanoparticles, which could prevent the particles from aggregation. The successful formulations of $\text{GaOOH}:\text{Cr}^{3+}$ and $\beta\text{-Ga}_2\text{O}_3:\text{Cr}^{3+}$ nanoparticles were also confirmed by the X-ray powder diffraction (XRD) measurements, in which the diffraction peaks of $\text{GaOOH}:\text{Cr}^{3+}$ and $\beta\text{-Ga}_2\text{O}_3:\text{Cr}^{3+}$ were similar with those of JCPDS 06-0180 and JCPDS 41-1103, respectively (Figure 1C).

Preparation and characterization of anti-ICAM-TPGS/ $\beta\text{-Ga}_2\text{O}_3:\text{Cr}^{3+}$ /TIG

In the following section, $\beta\text{-Ga}_2\text{O}_3:\text{Cr}^{3+}$ nanoparticles loaded with tigecycline (TIG) were prepared using the anti-ICAM-TPGS as a capping

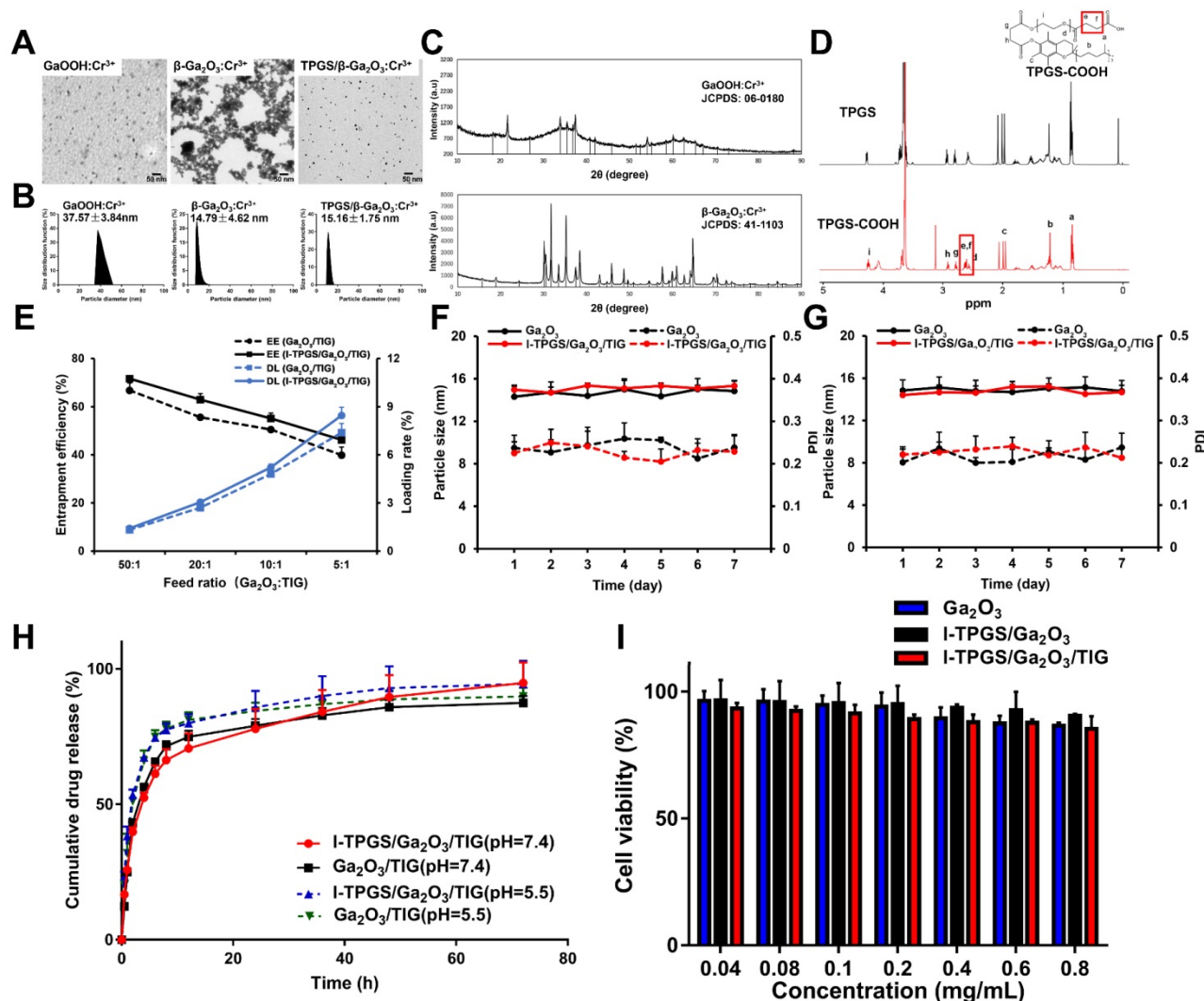


Figure 1. Preparation and characterization of anti-ICAM-TPGS/ $\beta\text{-Ga}_2\text{O}_3:\text{Cr}^{3+}$ /TIG. (A) TEM images of $\text{GaOOH}:\text{Cr}^{3+}$, $\beta\text{-Ga}_2\text{O}_3:\text{Cr}^{3+}$ and TPGS/ $\beta\text{-Ga}_2\text{O}_3:\text{Cr}^{3+}$ were taken. (B) The hydrodynamic particle size distribution (PSD) of $\text{GaOOH}:\text{Cr}^{3+}$ suspended in water, and PSD of $\beta\text{-Ga}_2\text{O}_3:\text{Cr}^{3+}$ nanoparticles suspended in water and TPGS solution were detected respectively by dynamic light scattering (DLS) at room temperature ($n=3$). (C) The X-ray powder diffraction (XRD) spectra of $\text{GaOOH}:\text{Cr}^{3+}$ and $\beta\text{-Ga}_2\text{O}_3:\text{Cr}^{3+}$ were carried out with a Cu K α radiation source in the 2θ ranging from 10° to 90° . (D) ^1H NMR spectra of TPGS and TPGS-COOH recorded in deuterated chloroform. (E) Loading rate and encapsulation efficiency of $\text{Ga}_2\text{O}_3/\text{TIG}$ and I-TPGS/ $\text{Ga}_2\text{O}_3/\text{TIG}$ nanoparticles under various feed ratios ($n=3$). (F) The stability of Ga_2O_3 and I-TPGS/ $\text{Ga}_2\text{O}_3/\text{TIG}$ nanoparticles in PBS ($n=3$). (G) The stability of Ga_2O_3 and I-TPGS/ $\text{Ga}_2\text{O}_3/\text{TIG}$ nanoparticles suspended in water ($n=3$). (H) The *in vitro* drug release behaviors of $\text{Ga}_2\text{O}_3/\text{TIG}$ and I-TPGS/ $\text{Ga}_2\text{O}_3/\text{TIG}$ nanoparticles in PBS (pH 5.5 or 7.4) at 37°C under shaking (75 rpm) ($n=3$). (I) Cytotoxicity of Ga_2O_3 , I-TPGS/ Ga_2O_3 and I-TPGS/ $\text{Ga}_2\text{O}_3/\text{TIG}$ nanoparticles against HUEVC after 48 h incubation performed by MTT assay ($n=3$).

agent. For convenience, the prepared β -Ga₂O₃:Cr³⁺, anti-ICAM-TPGS/ β -Ga₂O₃:Cr³⁺ were abbreviated as Ga₂O₃ and I-TPGS/Ga₂O₃, respectively. TPGS was firstly treated with the succinic anhydride to obtain the TPGS-COOH. ¹H-NMR spectrums displayed that TPGS-COOH had the characteristic peaks of TPGS, but also had two new peaks emerging at 2.63 ppm and 2.66 ppm, respectively (Figure 1D). Apparently, the two peaks belonged to the methylene groups of succinic acid attaching onto the TPGS molecules, which suggested that TPGS was successfully converted into TPGS-COOH. Then, the anti-ICAM-TPGS could be easily obtained by conjugating TPGS-COOH with ICAM-1 antibody via condensation reaction. The conjugation efficiency of ICAM-1 antibody to TPGS/Ga₂O₃ has been measured via micro BCA protein assay, which was determined to be 84.92%. Similar to TPGS/Ga₂O₃, I-TPGS/Ga₂O₃ also had the average particle size of around 15 nm, indicating that the conjugations of ICAM-1 antibody onto TPGS had little impact on the stabilization of Ga₂O₃ (Figure S1).

Herein, TIG was chosen as a model drug because it is widely used for the treatment of *Klebsiella pneumoniae* infection. From our previous research on Ga₂O₃ nanoparticles [17, 29], it was shown that the Ga₂O₃ obtained by calcination of GaOOH will form a pore structure, which may be due to the surface collapse of the nanoparticles caused by the loss of hydroxyl groups during calcination. Therefore, we can take advantage of the pore structure on the surface of Ga₂O₃ nanoparticles to encapsulate drugs. The TIG was then entrapped in the Ga₂O₃ by adsorption. By increasing the feed ratio of Ga₂O₃ to TIG from 50:1 to 5:1, both Ga₂O₃ and I-TPGS/Ga₂O₃ exhibited similar behaviors, showing decreases in the encapsulation efficiency (EE), but increases in drug loading (DL) for TIG (Figure 1E). This result demonstrated that the modification of anti-ICAM-TPGS had few effects on the EE and DL of Ga₂O₃ nanoparticles. We chose the I-TPGS/Ga₂O₃/TIG prepared with Ga₂O₃: TIG ratio of 5:1 in the following experiments because they had relative high drug loading capacity of 8.46 ± 0.51 %. The particle size of I-TPGS/Ga₂O₃/TIG was determined to be 15.33 ± 1.26 nm, indicating that the TIG loading had no significant effect on the particle size of the formulation. The stability of Ga₂O₃ and I-TPGS/Ga₂O₃/TIG was conducted in PBS and water, respectively. As shown in Figures 1F&G, the particle size and PDI of Ga₂O₃ and I-TPGS/Ga₂O₃/TIG nanoparticles did not change significantly within 7 days, indicating that the nanoparticles were well stabilized in PBS and water. As shown in Figure 1H, I-TPGS/Ga₂O₃/TIG and Ga₂O₃/TIG had similar drug

release behaviors, with the encapsulated TIG quickly releasing from the nanoparticles during the initial periods of 10 h, followed by prolonged sustained releases through 72 h. Morphology observation of I-TPGS/Ga₂O₃/TIG before and after the pH 5.5 drug release study was conducted and the morphology of I-TPGS/Ga₂O₃/TIG TEM did not presented significantly change (Figure S2). Drug release profiles also revealed that the TIG release from I-TPGS/Ga₂O₃/TIG and Ga₂O₃/TIG was pH-independent, since their drug release behaviors at pH 7.4 were quite similar with that of pH 5.5 (Figure 1H), meaning the acidic environment of the inflammatory infection site (pH 5.5) [30, 31] did not significantly affect the release behavior, which allowed us to ensure the normal drug release behavior of the nanoparticles.

The cytotoxicity of nanoparticles (Ga₂O₃, Ga₂O₃/TIG, and I-TPGS/Ga₂O₃/TIG) towards human umbilical endothelial vein (HUEVC) cells was evaluated via MTT assay. The results suggested that all of the nanoparticles had very low toxicities to HUEVC, as reflected by the observation that most of the cells (> 85%) were survival even when the concentrations used were up to 0.8 mg/mL (Figure 1I). The low toxicity of nanoparticles towards normal cells suggested they could be further applied in the following experiments.

Antibacterial studies

After the encapsulation of TIG, the antibacterial activities of I-TPGS/Ga₂O₃/TIG against TIG-sensitive *Klebsiella pneumoniae* (KPN) and TIG-resistant *Klebsiella pneumoniae* (TRKP) were subsequently investigated, and those treated with free TIG were applied as control groups. We found that the minimum inhibitory concentrations (MIC) and minimum bactericidal concentrations (MBC) of free TIG, Ga₂O₃/TIG and I-TPGS/Ga₂O₃/TIG on KPN bacteria were quite similar, which were around 0.3 μ g/mL and 0.6 μ g/mL, respectively (Figures 2A&B). The *in vitro* antibacterial study of free I-TPGS and unloaded Ga₂O₃ were also studied and the results showed that both of these two formulations did not show significant antibacterial activity against both KPN and TRKP bacteria. Their MICs on both bacteria exceeded 1 mg/mL. These results indicated that the three preparations studied had similar antibacterial efficacy in term of inhibiting the growth of KPN. In contrast, the antibacterial activities of the three preparations towards TRKP were quite different. It was found that both of Ga₂O₃/TIG and free TIG groups showed similar MIC and MBC values of about 1.8 μ g/mL and 3.6 μ g/mL, respectively. However, the MIC and MBC values of the I-TPGS/Ga₂O₃/TIG nanoparticles were

greatly reduced to 0.6 $\mu\text{g/mL}$ and 1.2 $\mu\text{g/mL}$, respectively. The results indicated that the antibacterial activity of $\text{Ga}_2\text{O}_3/\text{TIG}$ towards TRKP could be significantly improved by using the anti-ICAM-TPGS as a surfactant, further achieving the overcoming of the drug resistance to some extent. The antimicrobial activity of TIG in the presence of TPGS has also been studied and the results (Figure S3) also indicated a significantly improved antibacterial activity towards TRKP and the ability to overcome drug resistance with the presence of TPGS.

We also observed and recorded growth curves of the three preparations on the growth of KPN and TRKP strains. In the case of KPN, free TIG, $\text{Ga}_2\text{O}_3/\text{TIG}$ and I-TPGS/ $\text{Ga}_2\text{O}_3/\text{TIG}$ at a TIG concentration of 0.15 $\mu\text{g/mL}$ could not restrain the bacterial growth because their CFU/mL values were remarkably increased after 22 h of incubation (Figure 2C). By increasing the concentration of TIG to 0.3 $\mu\text{g/mL}$, all of the three preparations exhibited slight change in CFU/mL values during incubation for 22 h, meaning that they were effective at inhibiting the bacterial growth at the TIG concentration of 0.3 $\mu\text{g/mL}$ (Figure 2C). These results were consistent with the results in Figures 2A&B, demonstrating that TIG concentration had a considerable similar impact on the antimicrobial activity towards KPN, regardless

of carrier type. In the case of TRKP, only I-TPGS/ $\text{Ga}_2\text{O}_3/\text{TIG}$ at a TIG concentration of > 0.6 $\mu\text{g/mL}$ was able to prevent the bacteria from growth, showing slight increases of CFU/mL after 22 h of incubation, while TIG, $\text{Ga}_2\text{O}_3/\text{TIG}$ at a TIG concentration of 1.2 $\mu\text{g/mL}$ failed to inhibit the growth trend of TRKP (Figure 2D). These results were also consistent with the results in Figures 2A&B. Overall, I-TPGS/ $\text{Ga}_2\text{O}_3/\text{TIG}$ had much stronger antibacterial activity than $\text{Ga}_2\text{O}_3/\text{TIG}$ and free TIG, revealing the ability to inhibit the drug-resistant TRKP from growth.

One possible reason for the enhanced antimicrobial activity towards TRKP of I-TPGS/ $\text{Ga}_2\text{O}_3/\text{TIG}$ could be due to the fact that I-TPGS/ $\text{Ga}_2\text{O}_3/\text{TIG}$ had more uniform particle distributions, which could be easier for the particles to go through the cell wall of bacteria and deliver TIG. Previous studies have suggested that TPGS has the ability to overcome anticancer drug-resistance by efflux pump inhibition and endocytosis promotion [18, 30, 32]. We supposed that TPGS could also inhibit the activity of bacterial efflux pumps, thereby leading to an enhanced antimicrobial activity towards TRKP. In order to prove our hypotheses, we carried out the following experiments.

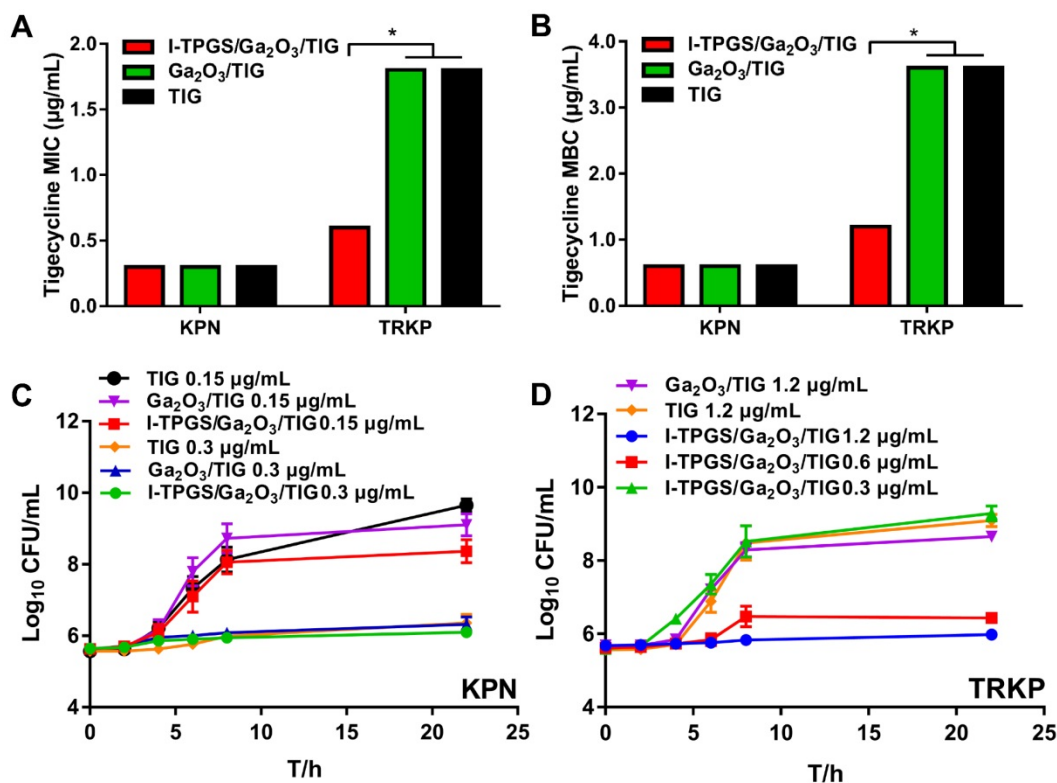


Figure 2. *In vitro* antibacterial studies of I-TPGS/ $\text{Ga}_2\text{O}_3/\text{TIG}$ and control samples on KPN and TRKP. (A) MIC susceptibility semiquantitative profiles of TIG, $\text{Ga}_2\text{O}_3/\text{TIG}$ and I-TPGS/ $\text{Ga}_2\text{O}_3/\text{TIG}$ against KPN and TRKP using microplate broth dilution method (n=3). (B) MBC susceptibility semiquantitative profiles of TIG, $\text{Ga}_2\text{O}_3/\text{TIG}$ and I-TPGS/ $\text{Ga}_2\text{O}_3/\text{TIG}$ against KPN and TRKP (n=3). (C) Growth curves for KPN treated with various concentrations of TIG, $\text{Ga}_2\text{O}_3/\text{TIG}$ or I-TPGS/ $\text{Ga}_2\text{O}_3/\text{TIG}$ (n=3). (D) Growth curves for TRKP treated with various concentrations of TIG, $\text{Ga}_2\text{O}_3/\text{TIG}$ or I-TPGS/ $\text{Ga}_2\text{O}_3/\text{TIG}$ (n=3), *p<0.05.

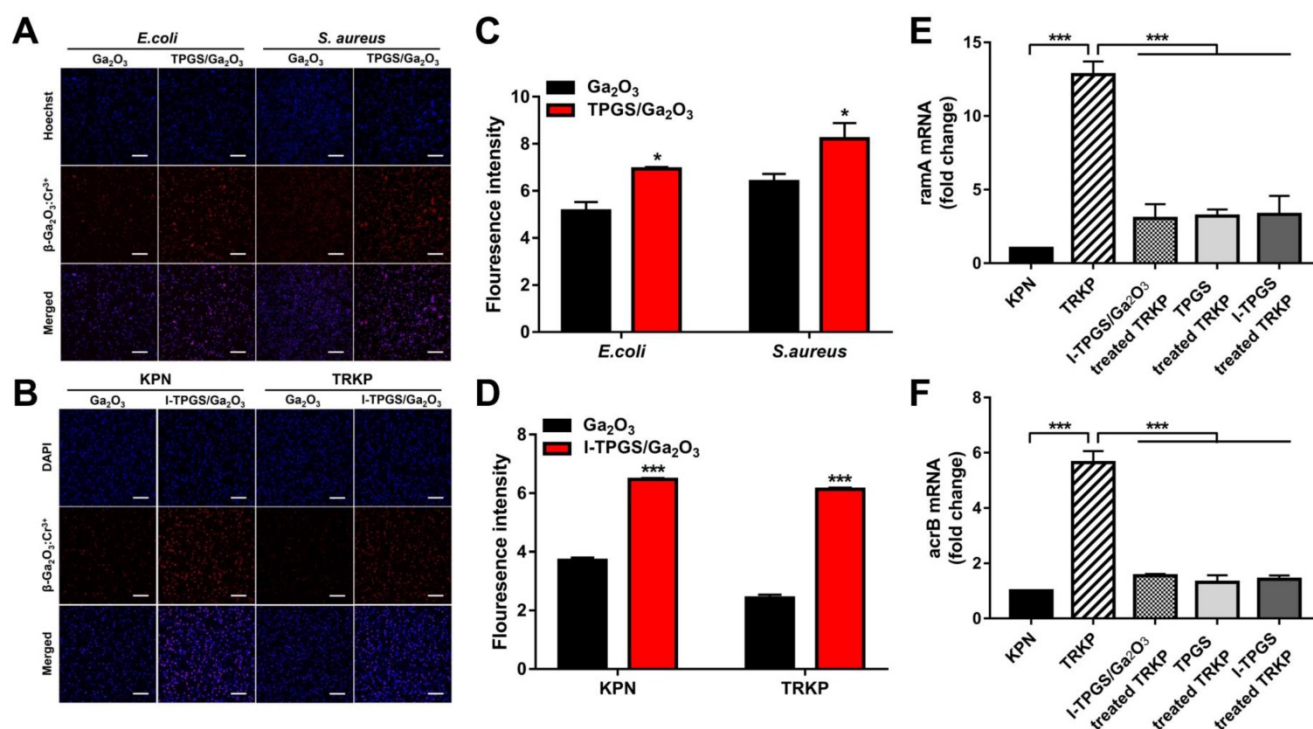


Figure 3. Investigation on mechanisms of I-TPGS/Ga₂O₃ overcoming drug resistance. (A) The fluorescent images and (C) semi-quantitative analysis (n=3) of fluorescence intensity of β -Ga₂O₃:Cr³⁺ after *E. coli* or *S. aureus* was incubated with Ga₂O₃ and TPGS/Ga₂O₃ for 4 h at 37 °C, respectively. The bacteria were labelled with Hoechst (blue), and the red fluorescence signal indicated the excited red fluorescence from β -Ga₂O₃:Cr³⁺. The scale bar is 20 μ m. (B) The fluorescent images and (D) semi-quantitative analysis (n=3) of fluorescence intensity of β -Ga₂O₃:Cr³⁺ after KPN or TRKP was treated with Ga₂O₃ and I-TPGS/Ga₂O₃ for 4 h at 37 °C, respectively. The bacteria were labelled with DAPI (blue), and the red fluorescence signal indicated the excited red fluorescence from β -Ga₂O₃:Cr³⁺. The scale bar is 20 μ m. (E&F) After TRKP was treated with I-TPGS, I-TPGS/Ga₂O₃ and TPGS for 20 h at 37 °C, respectively (n=3). The expression levels of (E) ramA and (F) acrB mRNA transcripts of I-TPGS/Ga₂O₃ treated TRKP, I-TPGS treated TRKP and TPGS treated TRKP were assessed by RT-PCR method. Untreated KPN and TRKP were used as control. *p<0.05, **p<0.01, ***p<0.001. The error presents the standard deviation from the mean.

Investigation on mechanisms of overcoming drug resistance

Fluorescence confocal imaging

In order to the mechanism of the enhanced antibacterial activity of I-TPGS/Ga₂O₃/TIG towards KPN and TRKP, the behavior of nanoparticles being transported into bacteria and their effects on efflux pumps in resistant bacteria were further studied.

Firstly, *Escherichia coli* (*E. coli*) and *Staphylococcus aureus* (*S. aureus*) were selected as representative strains of Gram-negative bacteria and Gram-positive bacteria, respectively. Ga₂O₃ with small particle size and uniform distribution was prepared with TPGS capping to investigate their transportation into bacteria considering small particles were supposed to cross the cross-linked cell wall barrier easier. Ga₂O₃ was applied as control. The bacteria were labelled by Hoechst (blue), while the Ga₂O₃ doped with Cr³⁺ could excite fluorescence as a fluorescent probe at an excitation wavelength of 635 nm (red). The observable fluorescent signals of β -Ga₂O₃:Cr³⁺ in Figures 3A&C proved that Ga₂O₃ could be internalized into both of Gram-negative bacteria and Gram-positive bacteria after 4 h of incubation at 37 °C. Furthermore, the presented stronger fluorescent intensity of

β -Ga₂O₃:Cr³⁺ in TPGS/Ga₂O₃ treated bacteria indicated that nanoparticles with a better dispersion were more readily internalized. Then, the bacterial uptake of I-TPGS/Ga₂O₃/TIG was further investigated on KPN and TRKP. The results showed that both of Ga₂O₃ and I-TPGS/Ga₂O₃/TIG could be taken up by KPN and TRKP after 4 h of incubation at 37 °C, and the fluorescent signal of I-TPGS/Ga₂O₃/TIG nanoparticles in bacteria was significantly enhanced compared with that of Ga₂O₃ (Figures 3B&D). The results indicated that small-sized monodispersed nanoparticles were more easily to be internalized into the bacteria, thereby facilitating the intra-bacterial delivery of antibiotics.

Real-time RT-PCR

Then, the effect of I-TPGS/Ga₂O₃/TIG on the efflux pumps on TRKP was evaluated by measuring the expression level of efflux pumps-related genes via real-time RT-PCR method. Previous studies have reported that efflux pump gene (*acrB*) and transcriptional activator (*ramA*) could up-regulate the activity of multidrug efflux pump AcrAB in drug-resistant *Klebsiella pneumoniae*, thus promoting the antibiotic resistance [20, 33]. The bacterial cultures of KPN and TRKP harvested in the mid-exponential

growth phase were incubated with TPGS, I-TPGS and I-TPGS/Ga₂O₃ for 20 h at 37 °C, respectively. As shown in Figures 3E&F, the expression levels of ramA and acrB in untreated TRKP were up-regulated by 12.8-fold and 5.6-fold compared with their expression levels in KPN, which confirmed that the overexpression of acrB and ramA were involved in the TIG resistance in TRKP. After treating with I-TPGS/Ga₂O₃/TIG, the expression levels of ramA and acrB in TRKP were down-regulated by about 4.3-fold and 3.6-fold, respectively. Similar trends were presented in the results of TPGS treated TRKP group and I-TPGS treated TRKP group, indicating that the presence of TPGS in I-TPGS/Ga₂O₃ played an important role in the inhibition of efflux pump genes. Although the expression levels of these two genes in TRKP were still higher than those of KPN, the significantly down-regulated gene expression levels still highlighted that I-TPGS/Ga₂O₃/TIG were able to inhibit the activity of efflux pumps in resistant bacteria to a large extent and posed a great potential to overcome bacterial resistance. In this way, the increased distribution of the antibiotic-loaded nanoparticles in the bacteria along with the reduced efflux of the loaded antibiotics could effectively overcome the drug-resistance in bacteria and restore the sensitivity of bacteria to antibiotics.

Cellular uptake study

In addition to inhibiting the bacterial efflux pump by the modification of TPGS, the targeting specificity of I-TPGS/Ga₂O₃ was also of particular

concern, which was first evaluated *in vitro* using Human umbilical endothelial vein (HUEVC) cells. HUEVC was stimulated with LPS for 24 h to simulate the pathological endothelium state of the cells in the infected sites. Western blot analysis revealed there was a significant increase in the expression level of ICAM1 in LPS-incubated HUEVC (Figures 4A&B), suggesting that pathological endothelium of HUEVC with over-expressed ICAM1 was successfully established. To conduct the cellular uptake studies, HUEVC with or without LPS pretreatment were incubated with Ga₂O₃ and I-TPGS/Ga₂O₃ for 2, 4 and 8 h, respectively. Fluorescent images of HUEVC incubated with I-TPGS were also observed as a reference (Figure S4). ICAM1 blockage experiment was also conducted to further investigate the endocytosis of I-TPGS/Ga₂O₃. The cells were labelled with DAPI (red), and Ga₂O₃ (β-Ga₂O₃:Cr³⁺) could excite fluorescence as a fluorescent marker (blue). It was observed that the cellular uptake behaviors of I-TPGS/Ga₂O₃ and Ga₂O₃ were time-dependent in all the groups (Figures 4C&D). The results also revealed that the fluorescent signal in HUEVC treated with I-TPGS/Ga₂O₃ was stronger than that treated with Ga₂O₃, which could be owing to the improved dispersibility and stability of nanoparticles after I-TPGS modification. We also observed that the pretreatment of LPS resulted in a significantly increased fluorescence intensity of I-TPGS/Ga₂O₃ (Figures 4C&D). Given the fact that LPS incubation could result in an increased expression of ICAM1, the reason could be related to the specific binding

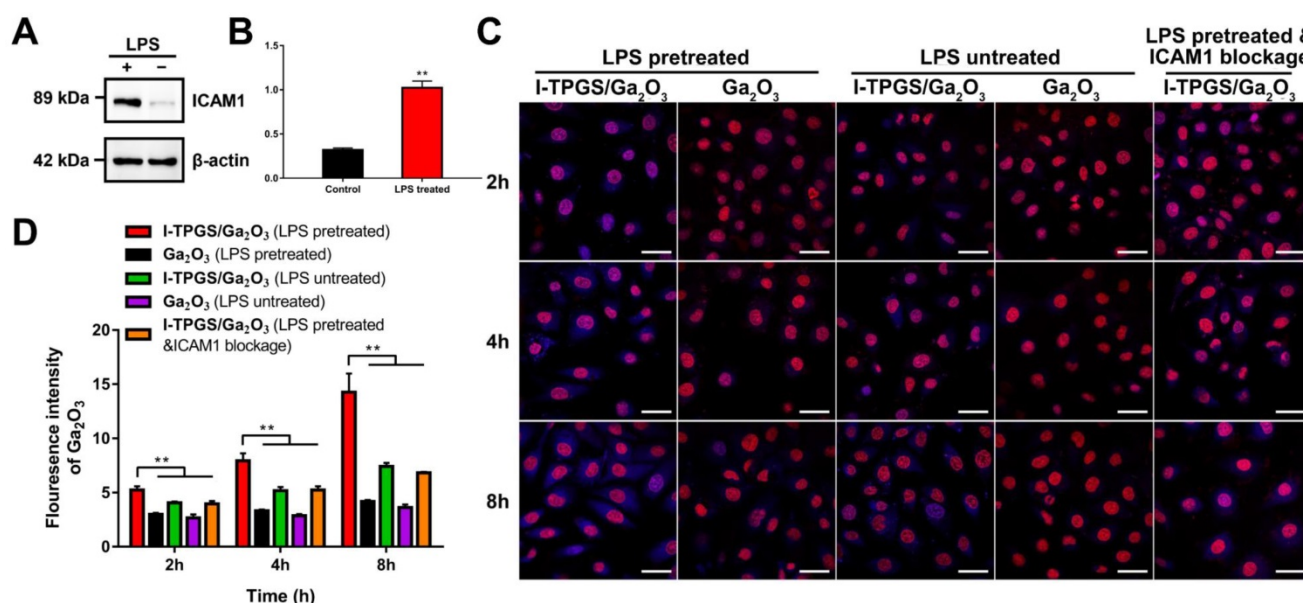


Figure 4. Cellular uptake study. (A) Western blot analysis of ICAM1 expression in LPS pretreated HUEVC (ICAM1 highly expressing) and untreated HUEVC (ICAM1 lowly expressing) cells. (B) Semi-quantitative analysis of expression levels of ICAM1 in LPS treated group and control group (n=3). (C) The cellular fluorescent uptake images and (D) semi-quantitative analysis (n=3) of fluorescence intensity of Ga₂O₃ or I-TPGS/Ga₂O₃ incubated with HUEVC for 2 h, 4 h and 8 h in the presence or absence of LPS pretreatment and ICAM1 blockage, respectively. HUEVC were labelled with DAPI (red), and the blue fluorescence signal indicated the excited blue fluorescence from β-Ga₂O₃:Cr³⁺. The bar is 40 μm. **p<0.01.

between the ICAM1 antibody on the surface of I-TPGS/Ga₂O₃ and ICAM1 adhesion molecules on the cell surface under inflammatory pathological state. In addition, the uptake of I-TPGS/Ga₂O₃ was significantly reduced after the ICAM1 blockage, which further confirmed that the specific interaction between I-TPGS/Ga₂O₃ and ICAM1 epitopes could contribute to a higher internalization (Figures 4C&D). The targeting specificity and enhanced cellular internalization of I-TPGS/Ga₂O₃ were of great significance to increase the effective concentration of antibiotics in the infected sites and to treat the intracellular infections more effectively.

In vivo biodistribution study

Then, the targeting specificity of I-TPGS/Ga₂O₃ was further investigated *in vivo*. Other than a drug carrier, I-TPGS/Ga₂O₃ could also be applied as a fluorescence probe here to observe its *in vivo* biodistribution after doping Cr³⁺ into β-Ga₂O₃ (Figure 5A). Herein, the acute pneumonia mouse model was established by injecting KPN and TRKP bacteria into

the lungs of healthy mice *via* trachea. After intravenous administration, *in vivo* biodistribution of I-TPGS/Ga₂O₃ was observed at 5 h and 24 h, respectively. Ga₂O₃ and TPGS/Ga₂O₃ were used as control groups. The results indicated an increased fluorescent signal of I-TPGS/Ga₂O₃ in the lungs from 5 h to 24 h in both acute KPN-infected and TRKP-infected pneumonia mice. The strongest fluorescent signals (counts/g) in lungs presented a significantly increased accumulation in all of the collected tissues of I-TPGS/Ga₂O₃ treated mice (Figures 5B-E). At the meantime, Ga₂O₃ and TPGS/Ga₂O₃ treated mice failed to present a most accumulation in lungs other than other tissues. Obviously, a stronger fluorescent signal was always presented in the lungs of I-TPGS/Ga₂O₃ treated mice compared to that in lungs of Ga₂O₃ or TPGS/Ga₂O₃ treated mice, indicating an increased nanoparticles accumulation in the infected site via targeted delivery (Figures 5B-E). At the same time, the immunohistochemical results showed high expression of ICAM1 in the lungs of acute pneumonia

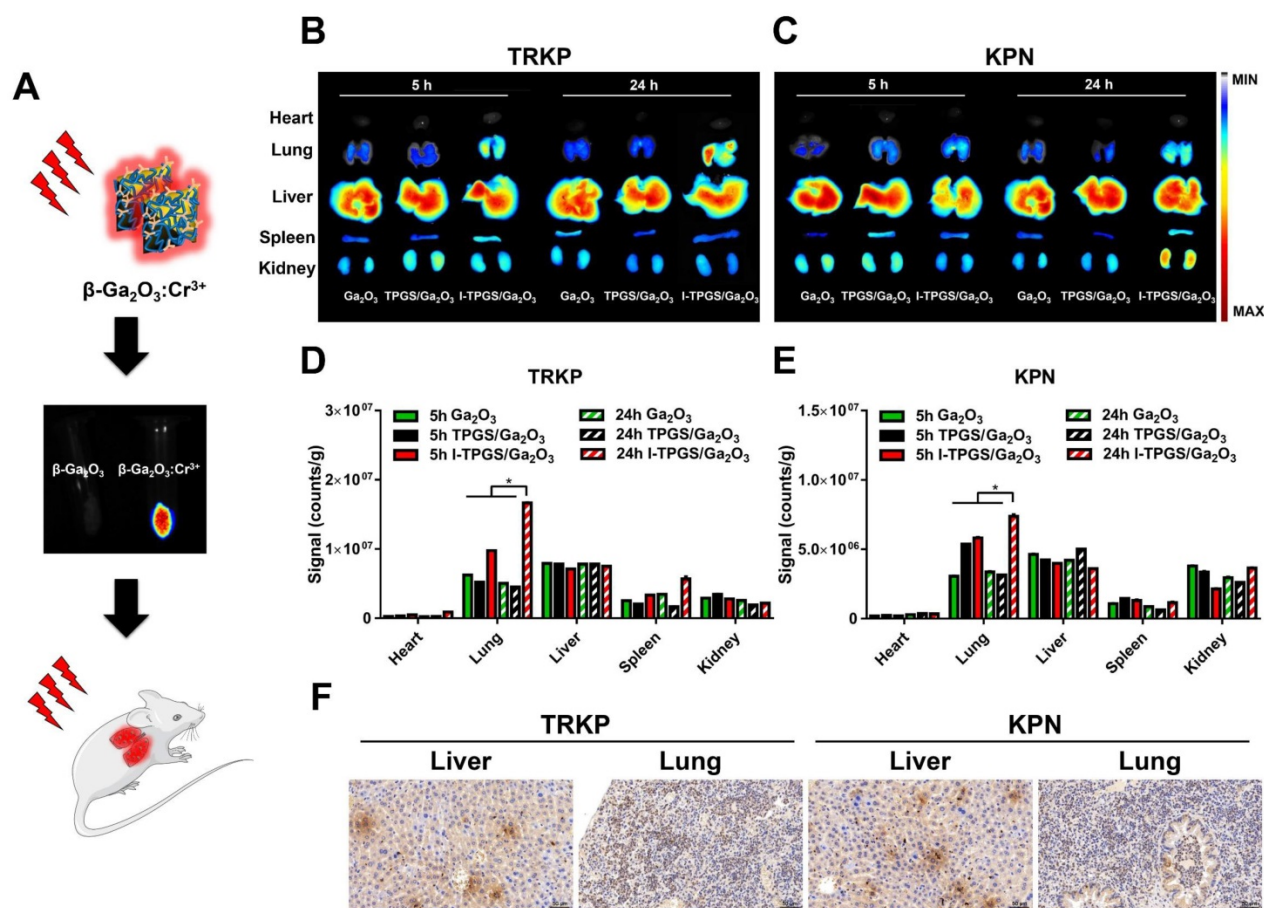


Figure 5. In vivo biodistribution study. (A) Schematic illustration for the procedure of β-Ga₂O₃ doped with Cr³⁺ used for bioimaging at an excitation wavelength of 635 nm. (B) The *in vivo* fluorescence images and (D) semi-quantified fluorescence signals (total signal/counts of the fluorescence signal per gram of tissue) of collected tissues from acute TRKP-infected pneumonia mice at 5 h, 24 h after intravenous injection with Ga₂O₃, TPGS/Ga₂O₃ and I-TPGS/Ga₂O₃. (C) The *in vivo* fluorescence images and (E) semi-quantified fluorescence signals (total signal/counts of the fluorescence signal per gram of tissue) of collected tissues from acute KPN-infected pneumonia mice at 5 h, 24 h after intravenous injection with Ga₂O₃, TPGS/Ga₂O₃ and I-TPGS/Ga₂O₃. (n=4) (F) Immunohistochemical analysis of livers and lungs from acute TRKP-infected and KPN-infected pneumonia mice using immunohistochemical staining for ICAM1 after 24 h of injection. The magnification was 200 times. *p<0.05.

mice after 24 h of injection, which suggested a specific delivery of I-TPGS/Ga₂O₃ into infected lung via the mediation of ICAM1 (Figure 5F). Meanwhile, a small amount of ICAM1 expression was also observed in the liver of these mice, so that I-TPGS/Ga₂O₃ could also be delivered to the liver to form a certain accumulation as reflected by the results of biodistribution study (Figure 5F). To sum up, bioimaging and lung targeting characteristic of I-TPGS/Ga₂O₃ were suggested here. And the targeted drug delivery by I-TPGS/Ga₂O₃ could effectively increase the concentration of antibiotics at the infected site at the same dose to achieve a better therapeutic effect.

In vivo anti-infective efficacy assessments

After confirming that I-TPGS/Ga₂O₃/TIG could exert enhanced antibacterial activity *in vitro*, further effectively overcome bacterial resistance and possess a targeting specificity to the site of infection *in vivo*, the *in vivo* anti-infective activities were eventually evaluated using an acute pneumonia mouse model. After 5 hours of modelling, the mice were intravenously injected with different formulations (saline, free TIG, Ga₂O₃/TIG and I-TPGS/Ga₂O₃/TIG) (Figure 6A). Then, the survival rate, body weight and counts of lung colonies were recorded within 5 days (Figures 6B&C, Figure S5). After treating with the same concentration of bacteria, the survival rate of

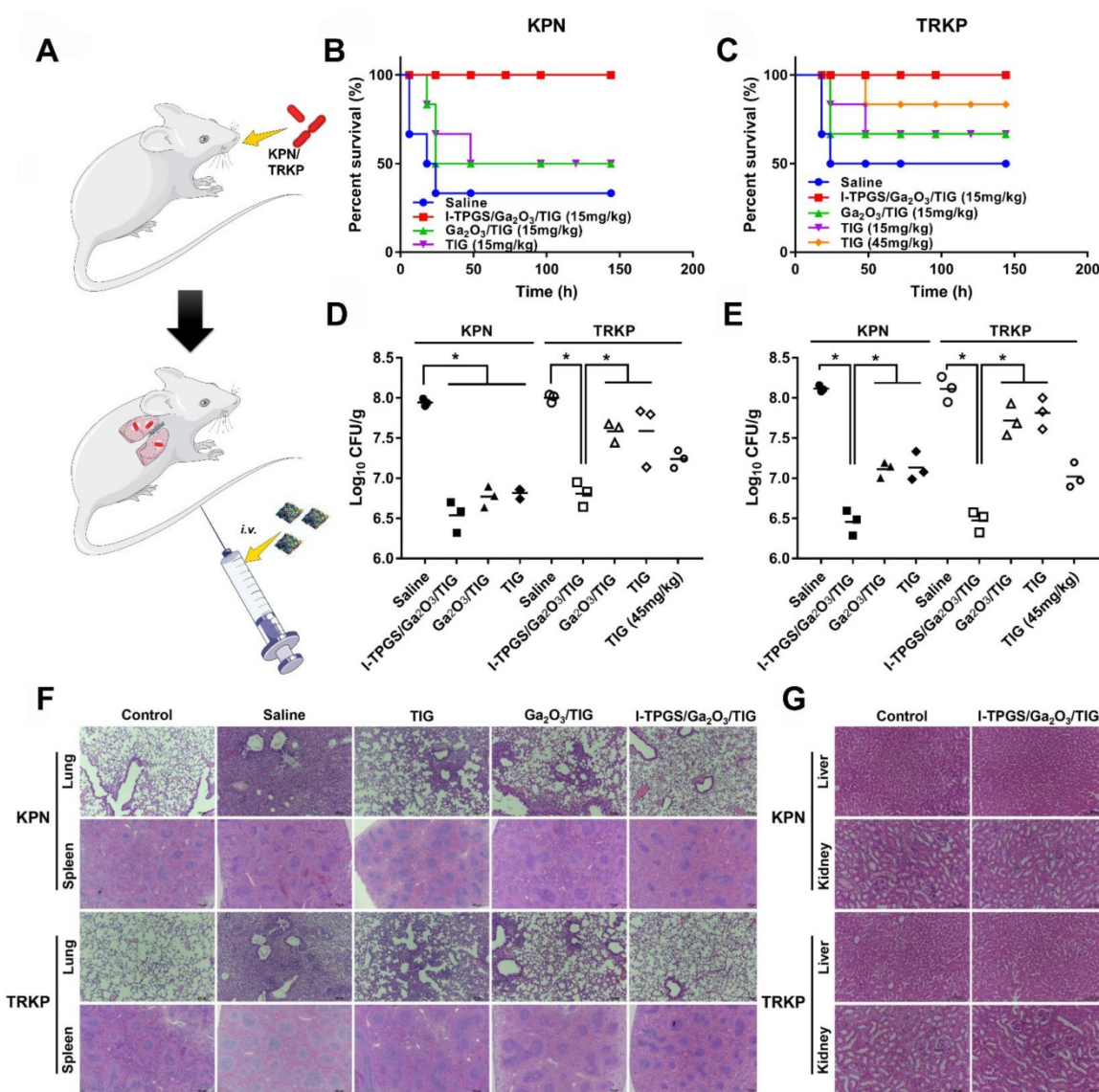


Figure 6. *In vivo* anti-infective efficacy assessments. (A) Schematic illustration for the procedure of the construction and treatment of the acute pneumonia mouse model. (B) Survival rates of acute KPN-infected pneumonia mice after treatments with saline, TIG, Ga₂O₃/TIG and I-TPGS/Ga₂O₃/TIG with a dose of 15 mg/kg, respectively. (n=6). (C) Survival rates of acute KPN-infected pneumonia mice after treatments with saline, TIG (15 mg/kg and 45 mg/kg), Ga₂O₃/TIG (15 mg/kg) and I-TPGS/Ga₂O₃/TIG (15 mg/kg), respectively. (n=6). (D&E) 48 h after the treatments, bacterial counts analysis in the lungs of acute (D) KPN-infected and (E) TRKP-infected pneumonia mice (n=3). (F) H&E staining images of lung and spleen of acute KPN-infected and TRKP-infected pneumonia mice after 48 h of treatments. The magnifications of lungs and spleens were 100 times and 40 times, respectively. (G) H&E staining images of liver and kidney of acute KPN-infected and TRKP-infected pneumonia mice after 5 days of I-TPGS/Ga₂O₃/TIG treatment, healthy mice were used as control. The magnification was 200 times. Scale bar = 100 μm. *p<0.05.

TRKP-infected pneumonia mice was slightly higher than that of the acute KPN-infected pneumonia mice, which could be explained as the virulence of the bacteria decreased with the acquisition of drug resistance [34, 35]. In these treatment groups, only I-TPGS/Ga₂O₃/TIG treated mice showed 100% of survival rate against KPN and TRKP infections (Figures 6B&C). Combined with previous results, the significantly improved treatment effect could be attributed to the ICAM1-mediated targeting delivery and TPGS-mediated better dispersibility, which allowed TIG-loaded nanoparticles to accumulate in the infected lungs and be endocytosed into epithelial cells, further achieving increased drug concentration and effective treatment of intracellular infections. Additionally, the survival rate of acute TRKP-infected pneumonia mice treated with 45 mg/kg of free TIG was 83.33%, which was still lower than that of groups treated with only 15 mg/kg of I-TPGS/Ga₂O₃/TIG (Figure 6C). The results suggested that the therapeutic effect of TIG could be greatly improved by loading TIG into I-TPGS/Ga₂O₃ nanoparticles, even when it was applied to drug-resistant infection. The previously demonstrated inhibited efflux pumps activity in TRKP mediated by TPGS capping could explain the superior performance of I-TPGS/Ga₂O₃/TIG in treating drug-resistant bacterial infections.

The body weights of the mice were first decreased and then increased, and the minimum weight value was occurred at 48-72 h (Figure S2), indicating that the animals were gradually recovered after 48-72 h of treatment. The colony counts in lungs of these mice were therefore performed at 24 h and 48 h, respectively. In general, I-TPGS/Ga₂O₃/TIG exhibited excellent performance in the treatment of bacterial infections (Figures 6D&E). All of the treatment groups showed a decrease in the number of lung colonies after 24 h of administration, which demonstrated the antibacterial effect of the treatments. The number of lung colonies in the I-TPGS/Ga₂O₃/TIG group was significantly lower than that in other treatment groups (Figure 6D). After 48 h, the number of lung colonies in the TIG and Ga₂O₃/TIG groups were increased, while that of I-TPGS/Ga₂O₃/TIG group still remained at a low level (Figure 6E). Similar results were also found in the KPN-infected mice, demonstrating the superior ability of I-TPGS/Ga₂O₃/TIG to combating microbial and antimicrobial efficacy and ability to overcoming drug resistance. Previous studies have revealed that TPGS was able to inhibit efflux pumps in drug-resistant cancer cells [18, 19]. This work was the first time to apply TPGS in the inhibition of bacteria-resistant efflux pumps, which was further used to treat drug-resistant bacterial infections.

As shown in Figure 5F, the infected mice presented some typical pathological features including enlarged lymphoid nodules on spleen, thickened alveolar walls and leukocytes infiltration on infected lungs. Histological improvements were observed after the treatments with TIG, Ga₂O₃/TIG and I-TPGS/Ga₂O₃/TIG. The improvement in these pathological changes was most pronounced in the I-TPGS/Ga₂O₃/TIG group compared to the other treatment groups at the same dose (Figure 6F). In addition to the outstanding therapeutic effects, the *in vivo* biosafety of I-TPGS/Ga₂O₃/TIG was also one of the issues we should deeply concerned. Referring to the previous results of *in vivo* biodistribution, there were higher accumulation of I-TPGS/Ga₂O₃/TIG in liver and kidney than other organs. The H&E staining of liver and kidney were therefore conducted after treating acute KPN-infected and TRKP-infected pneumonia mice for 5 days with I-TPGS/Ga₂O₃/TIG at the applied dose. No observable pathological abnormalities or damages were found in the liver and kidney of the mice, which demonstrates that the use of I-TPGS/Ga₂O₃/TIG did not cause obvious side effect or damage to other normal organs during the antibacterial treatment (Figure 6G). After treating mice with saline and I-TPGS/Ga₂O₃/TIG respectively, the white blood cell (WBC) count, lymphocytes (Lymph) count, monocytes (Mon) count, neutrophilic granulocyte (Gran) count, red blood cell (RBC) count and haemoglobin (HGB) of the whole blood were then determined. The results (Table S1) showed that the injection of I-TPGS/Ga₂O₃/TIG did not have any significant effect on the haematology parameters of mice. Overall, *in vivo* results indicated that I-TPGS/Ga₂O₃ can be used as a safe and efficient antibiotic delivery system to achieve efficient treatment of drug-resistant bacterial infections.

Conclusion

In summary, we prepared I-TPGS/Ga₂O₃ nanoparticles as a novel potential platform to encapsulate the antibacterial drug of TIG for a safe and effective targeted therapy of TRKP pulmonary infection. The results suggested that TIG could be loaded within the nano-sized I-TPGS/Ga₂O₃ particles, which had a superior *in vitro* antibacterial activity against the TRKP and overcome the drug-resistance to a certain extent. The small particle size and uniform distribution enabled the I-TPGS/Ga₂O₃ nanoparticles to be more easily internalized into the bacteria. TPGS modification of the nanoparticles could down-regulate the over-expression of the efflux pump genes in TRKP. In this way, the distribution of the antibiotic-loaded nanoparticles increased with the decrease of efflux of the loaded antibiotics, which

could effectively overcome the drug-resistance in bacteria and restore the bacterial sensitivity to antibiotics. The *in vivo* and *in vitro* distribution studies presented that the conjugated ICAM1 antibody could specifically deliver I-TPGS/Ga₂O₃ to the infected sites. In addition, Ga₂O₃ could be used as a fluorescent probe because of its photoluminescence properties, thereby avoiding multiple steps of additional grafting of fluorescent probe onto the nanoparticles. Finally, we applied I-TPGS/Ga₂O₃ to treat the acute pneumonia mice caused by KPN and TRKP infection. The greatly increased survival rates, largely reduced number of lung colonies, and significantly improved degree of pathological changes observed in I-TPGS/Ga₂O₃/TIG treated groups suggested that I-TPGS/Ga₂O₃/TIG could provide a safe and effective treatment of drug-resistant bacterial infections. We innovatively applied TPGS to overcome bacterial resistance and targeted deliver antibacterial drugs to infected sites through the mediation of ICAM1 antibody, eventually providing a novel approach with great potential and application value for the treatment of drug-resistant bacterial infections. Additionally, I-TPGS/Ga₂O₃ can be further developed and applied it to the diagnosis and real-time monitoring of anti-infective treatments by virtue of their own fluorescent properties.

Methods

Materials

Gallium oxide (Ga₂O₃), D- α -Tocopherol polyethylene glycol 1000 succinate (TPGS1000), sodium acetate (NaAc), glacial acetic acid, hydrogen peroxide (H₂O₂, 30%), chromic nitrate nonahydrate (Cr(NO₃)₃·9H₂O) were purchased from Aladdin Chemistry Co. (Shanghai, China). Lipopolysaccharide (LPS), succinic anhydride, N-(3-Dimethylamino-propyl)-N'-ethylcarbodiimide hydrochloride (EDC), 4-Dimethylaminopyridine (DMAP), N-hydroxysuccinimide (NHS), 4', 6-diamidino-2-phenylindole (DAPI), Hoechst 33342 and 3-(4,5-dimethylthiazol-2-yl)-2,5-diphenyltetrazolium bromide (MTT) were purchased from Sigma-Aldrich Co., Ltd (USA). All of the other chemicals were of analytical or chromatographic grade.

Dulbecco's modified Eagle's medium (DMEM, high-glucose) with penicillin (100 U/mL) and streptomycin (100 U/mL) were purchased from Corning (USA).

Cell culture

Human umbilical endothelial vein (HUEVC) cells were obtained from the Institute of Biochemistry and Cell Biology (Shanghai, China) and then cultured in DMEM supplemented with 10% (v/v) fetal bovine

serum (FBS) with the environmental condition maintained at 37 °C in an atmosphere of 5% CO₂/95% O₂ with 90% relative humidity. The cells were sub-cultured regularly using trypsin/EDTA. Mouse anti-mouse Anti-ICAM1 antibody (ab171123) and rabbit anti-human ICAM1 antibody (ab53013) were purchased from Abcam (Cambridge, MA).

Escherichia coli ATCC 25922 (*E. coli*), *Staphylococcus aureus* ATCC 29213 (*S. aureus*), tige cycline non-susceptible *Klebsiella pneumonia* 5542 (TRKP) and tige cycline susceptible *Klebsiella pneumonia* 55388 (KPN) were obtained from the First Affiliated Hospital, School of Medicine, Zhejiang University in China. Bacterial identification was performed by the Vitek 32 system (bioMérieux, France). The isolates were cultivated on nutrient agar plates, then harvested and cultured in LB medium or MH medium at 37 °C, 180 rpm under aerobic conditions grown to an OD₆₀₀ of 0.5 ~ 0.6 that corresponds to the exponential phase.

Animals

All experiments were performed in compliance with guidelines set by the Zhejiang University Institutional Animal Care and Use Committee. All animal procedures were conducted in accordance with national regulations and approved by the local animal experiments ethical committee.

Preparation and characterization of β -Ga₂O₃:Cr³⁺ nanoparticles

β -Ga₂O₃:Cr³⁺ nanoparticles were synthesized by improved method described in our previous publication[17]. Briefly, GaCl₃ solution was prepared by dissolving an appropriate amount of Ga₂O₃ in HCl solution (4 M) through stirring and heating at 95 °C. The synthesis protocol of 20 mL reaction system was illustrated here: NaAc (0.48 g) was dissolved in 16 ml of ethanol solution (50%, v/v), and then 0.4 mL of GaCl₃ solution (0.8 M) was added under stirring. Next, glacial acetic acid was added dropwise until the cloudy mixture became transparent. Finally, 32 μ L of a chromium nitrate solution (0.1 M) was added, and the mixture was heated and stirred at 50 °C for 5 h. The volume of the total reaction system in this step could be expanded to 2 L, thereby the reaction capacity was greatly increased as compared with that of most other hydrothermal reactions which usually does not exceed 100 mL, and the reaction capacity of reactions carried out using the kettle will be much smaller. [27, 28] After completed reaction, the white precipitate was separated by centrifugation, and collected after being washed with deionized water for 3 times. After drying at 60 °C for 24 h, the Cr³⁺ doped gallium oxyhydroxide (GaOOH:Cr³⁺) was then

obtained. At last, the $\text{GaOOH}:\text{Cr}^{3+}$ was calcined at 600 °C for 3 h, and then calcined at 950 °C for another 3 h to obtain $\beta\text{-Ga}_2\text{O}_3:\text{Cr}^{3+}$ nanoparticles. The obtained nanoparticles were collected and dried under vacuum and stored in a four-degree refrigerator for further use.

The hydrodynamic particle size and morphology of $\text{GaOOH}:\text{Cr}^{3+}$ and $\beta\text{-Ga}_2\text{O}_3:\text{Cr}^{3+}$ were observed by Zetasizer (S90, Malvern Co., UK) and transmission electron microscopy (80kV, TEM; JEM-1200EX, JEOL, Japan), respectively. The crystal structure of $\text{GaOOH}:\text{Cr}^{3+}$ and $\beta\text{-Ga}_2\text{O}_3:\text{Cr}^{3+}$ were examined by X-ray powder diffraction (XRD) using a XRD (X' Pert PRO, Empyrean 200895, PANalytical B.V., the Netherlands).

Synthesis of TPGS-COOH

Firstly, TPGS-COOH was synthesized by activating TPGS with succinic anhydride (SA) via a ring opening reaction. Briefly, TPGS, SA and DMAP (1:2:1, mol/mol) was dissolved by adding an appropriate amount of anhydrous dioxane, and then allowed them to react at room temperature for 24 h under a nitrogen atmosphere. After that, the anhydrous dioxane was removed by rotary evaporation at 50 °C. The obtained crude product was then dissolved in 10 ml of ice-cold DCM, followed by passing through a filter (0.45 μm) to remove the unreacted SA. The filtrate was then allowed to precipitate in ethanol overnight at -20 °C. The precipitate was separated by centrifugation at 10,000 rpm for 10 min, and then TPGS-COOH was obtained by washing the precipitate with iced ethanol for 3 times. The structure of TPGS-COOH was confirmed $^1\text{H-NMR}$ method (Bruker AVIII 500 Mspectrometer, Fällanden, Switzerland).

Preparation of anti-ICAM-TPGS/ $\beta\text{-Ga}_2\text{O}_3:\text{Cr}^{3+}$ /TIG

The anti-ICAM-TPGS/ $\beta\text{-Ga}_2\text{O}_3:\text{Cr}^{3+}$ was prepared by conjugating ICAM1 antibody with TPGS-COOH/ $\beta\text{-Ga}_2\text{O}_3:\text{Cr}^{3+}$ via the amide reaction. In brief, TPGS-COOH/ $\beta\text{-Ga}_2\text{O}_3:\text{Cr}^{3+}$ was firstly prepared by dispersing 60 mg of $\beta\text{-Ga}_2\text{O}_3:\text{Cr}^{3+}$ nanoparticles into 10 mL of TPGS-COOH solution (3 mg/mL), followed by ultrasonication 5 min and centrifuging at 10000 rpm for 10 min. The TPGS-COOH/ $\beta\text{-Ga}_2\text{O}_3:\text{Cr}^{3+}$ precipitate was mixed with EDC and NHS (TPGS-COOH:EDC:NHS = 1:5:5, mol/mol) to activate the carboxyl group of TPGS-COOH at 37 °C for 15 min. The mixture was then centrifuged to collect the precipitate, which was then re-dispersed into water. Finally, the anti-ICAM-TPGS/ $\beta\text{-Ga}_2\text{O}_3:\text{Cr}^{3+}$ was obtained by putting 15 μg of ICAM1 antibody into the activated TPGS-COOH/ $\beta\text{-Ga}_2\text{O}_3:\text{Cr}^{3+}$ for 4 h via the

amide reaction. The prepared $\beta\text{-Ga}_2\text{O}_3:\text{Cr}^{3+}$ and anti-ICAM-TPGS/ $\beta\text{-Ga}_2\text{O}_3:\text{Cr}^{3+}$ were abbreviated as Ga_2O_3 and I-TPGS/ Ga_2O_3 , respectively. The I-TPGS/ Ga_2O_3 was separated by centrifugation at 12,000 rpm for 10 min, and then washed with deionized water for 3 times. Then the content of ICAM-1 antibody in the obtained I-TPGS/ Ga_2O_3 nanoparticles was determined using micro BCA protein assay, and TPGS/ Ga_2O_3 nanoparticles was applied as control. The hydrodynamic particle size and morphology of I-TPGS/ Ga_2O_3 were also examined by Zetasizer and TEM, respectively.

To prepare TIG-loaded Ga_2O_3 ($\text{Ga}_2\text{O}_3/\text{TIG}$), an appropriate amount of Ga_2O_3 was mixed with TIG solution (1 mg/mL), ultra-sonicated for 5 min, and then stirred overnight. As for the TIG-loaded I-TPGS/ Ga_2O_3 (I-TPGS/ $\text{Ga}_2\text{O}_3/\text{TIG}$), $\text{Ga}_2\text{O}_3/\text{TIG}$ was used to conjugate with ICAM1 antibody via the same protocol described above. The obtained $\text{Ga}_2\text{O}_3/\text{TIG}$ and I-TPGS/ $\text{Ga}_2\text{O}_3/\text{TIG}$ were collected by centrifugation and dried under vacuum and stored in a four-degree refrigerator for further use. The loading capacity and encapsulation efficiency was calculated by measuring the concentration of the free TIG collected in the supernatant via a UV-vis spectrophotometer (TU-1080, Beijing Purkinje General Instrument Co., Ltd., China) at a wavelength of 245 nm.

Characterization of anti-ICAM-TPGS/ $\beta\text{-Ga}_2\text{O}_3:\text{Cr}^{3+}$ /TIG

The *in vitro* drug release behaviors of $\text{Ga}_2\text{O}_3/\text{TIG}$ and I-TPGS/ $\text{Ga}_2\text{O}_3/\text{TIG}$ were evaluated in PBS (pH 5.5 and 7.4) via a dialysis bag method using PBS. The release medium was collected at predetermined time points, and then replaced with fresh PBS. The content of TIG was detected by High Performance Liquid Chromatography (HPLC) method to calculate the cumulative release percentage. The cytocompatibility of these formulations against HUEVC were performed using MTT method. The cell viabilities of Ga_2O_3 , I-TPGS/ Ga_2O_3 and I-TPGS/ $\text{Ga}_2\text{O}_3/\text{TIG}$ were then determined after the incubation with HUEVC under various concentration for 48 h respectively. Each measurement was conducted in triplicate.

Antibacterial studies

The *in vitro* antibiotic efficacy of free TIG, $\text{Ga}_2\text{O}_3/\text{TIG}$ nanoparticles and I-TPGS/ $\text{Ga}_2\text{O}_3/\text{TIG}$ nanoparticles against TIG-sensitive *Klebsiella pneumonia* (KPN) and TIG-resistant *Klebsiella pneumonia* (TRKP) were evaluated by measuring the minimal inhibitory concentration (MIC), minimum bactericidal concentration (MBC) and growth curves, respectively. The bacteria used in the study were

those harvested in the mid-exponential growth phase (absorbance at 620 nm was of 0.5 ~ 0.6). The MIC values of formulations (free TIG, Ga₂O₃/TIG, I-TPGS/Ga₂O₃/TIG, free I-TPGS and unloaded Ga₂O₃) were determined as the lowest concentration that completely inhibited bacterial growth after 20 h of incubation at 37 °C via microplate broth dilution method. For MBC tests, 50 µL of mixtures containing formulations and bacterial inoculum from the above MIC tests were incubated in agar plates for 24 h at 37 °C. MBC was taken as the lowest concentration of formulations that did not show any bacterial growth on the inoculated agar plates. As for the growth curves tests, the KPN and TRKP cultures were firstly diluted to a concentration of 5 × 10⁵ CFU/mL. Then, the KPN and TRKP were incubated (250 rpm, 37 °C) with free TIG, Ga₂O₃/TIG I-TPGS/Ga₂O₃/TIG at different concentrations. The absorbance of these cultures at different time intervals were detected at the wavelength of 620 nm, and the CFU counts were calculated relative to a standard curve of the CFU counts.

Fluorescence confocal imaging

Escherichia coli (*E. coli*) and *Staphylococcus aureus* (*S. aureus*) labelled with Hoechst 33342 were used as model strains. The bacteria harvested in the mid-exponential growth phase were incubated with either Ga₂O₃ or TPGS/Ga₂O₃ (final Ga₂O₃ concentration of 0.5 mg/mL) for 4 h. Then, the fluorescence signals of Hoechst and β-Ga₂O₃:Cr³⁺ were observed by a confocal fluorescence microscope (Olympus IX81-FV1000, Olympus, Tokyo, Japan), and then were semi-quantitatively analyzed with Image J. In another study, same procedures were performed on the DAPI-labelled TRKP and KPN, respectively.

Real-time RT-PCR

The Oligonucleotide primers of *acrB*, *ramA* and 16S rRNA (Sangon Biotech (Shanghai) Co., Ltd) were used for the real-time RT-PCR. The 16S rRNA gene was served as a reference gene. The bacterial cultures of KPN and TRKP harvested in the mid-exponential growth phase were incubated with TPGS, I-TPGS and I-TPGS/Ga₂O₃ (final TPGS and Ga₂O₃ concentrations were of 0.1 and 0.2 mg/mL, respectively) for 20 h at 37 °C, respectively. The DNase-treated RNA templates were then extracted from the treated bacterial cultures using RNAiso Plus. The concentrations of RNA were determined using a Nanodrop spectrophotometer (Thermo scientific, MA, USA). After that, the cDNA was synthesized by a PrimeScript RT-PCR kit (TaKaRa Bio). Finally, the expression levels of the *acrB* and *ramA* genes were determined by real-time reverse transcription-PCR (real-time RT-PCR) method

using a SYBR Premix Ex Taq kit (TaKaRa Bio) on an Applied Biosystems StepOnePlus Real-Time PCR system. Then the relative expression analysis of *acrB* and *ramA* were conducted using the 2^{-ΔΔCq} method.

Western Blot

HUEVC were firstly pretreated with LPS (final concentration of 400 ng/mL) for 24 h, and then the expression level of ICAM1 was measured by western blotting method. Briefly, HUEVC were lysed by lysis buffer (CellLytic M, Sigma-Aldrich, USA) and then centrifuged at 12000 rpm for 10 min to obtain the supernatant fraction. The enhanced BCA protein assay kit was then used to determine the concentration of protein present in the supernatant. The same amounts of denatured proteins were run in a 10% sodium dodecyl sulfate polyacrylamide gel electrophoresis, and transferred to a poly(vinylidene difluoride) membrane. For blocking the nonspecific sites, the poly(vinylidene difluoride) membrane was then infiltrated in bovine serum albumin (5%) for 1 h at room temperature. After incubation with the mouse anti-mouse Anti-ICAM1 antibody (1:2000) at 4 °C overnight, the goat anti-rabbit IgG (1:1000, Byotime Biotech, Jiangsu, China) secondary antibodies were applied to incubated with the washed membranes for 2 h at room temperature. β-actin was used as a control. The results of western blotting were visualized by the LI-COR Odyssey system (Lincoln, NE).

Cellular uptake study

Afterwards, I-TPGS, Ga₂O₃ and I-TPGS/Ga₂O₃ (final Ga₂O₃ concentration was of 0.2 mg/mL) were incubated with either LPS-pretreated or LPS-untreated HUEVC for 2, 4 and 8 h, respectively. Meanwhile, a blocking group was prepared by pretreating the HUEVC with free ICAM1 antibody (3 µg/mL) for 1h. HUEVC were labelled with DAPI. The fluorescent signal of DAPI and β-Ga₂O₃:Cr³⁺ were observed by a confocal fluorescence microscope, then the fluorescent signals were semi-quantitative analyzed with Image J.

In vivo biodistribution study

To build the acute KPN-infected and TRKP-infected acute pneumonia mouse models, 30 µL of KPN and TRKP (1×10⁹ CFU/mL) were injected into the lungs of healthy mice (female, 23 ± 2 g) via trachea. After intravenously injected Ga₂O₃, TPGS/Ga₂O₃ and I-TPGS/Ga₂O₃ (dose of Ga₂O₃ were 100 mg/kg), the organs (heart, lung, liver, spleen and kidneys) were collected at 5 and 24 h, respectively. The fluorescence signal of β-Ga₂O₃:Cr³⁺ accumulated in these tissues were observed and analyzed using the IVIS® spectrum system (Caliper, Hopkinton, MA,

USA). Immunohistochemistry analysis was further conducted on lungs and livers collected from sacrificed acute KPN-infected and TRKP-infected pneumonia mice after 24 h of administration.

In vivo anti-infective efficacy assessments

The *in vivo* antimicrobial activities of the formulations were evaluated by investigating the survival rates, body weights, and pathological changes. The treatments were carried out 5 h late after the modelling. The acute KPN-infected pneumonia mice were divided into four groups (n=6), and intravenously injected with saline, TIG, Ga₂O₃/TIG and I-TPGS/Ga₂O₃/TIG, respectively. The TIG content in each group was 15 mg/kg. On the other hand, the TRKP-infected pneumonia mice were divided into five groups (n=6), and intravenously injected with saline, TIG (15 mg/kg and 45 mg/kg), Ga₂O₃/TIG (TIG: 15 mg/kg) and I-TPGS/Ga₂O₃/TIG (TIG: 15 mg/kg), respectively. The survival rates and body weights of mice were evaluated within 5 days.

In addition, more healthy mice were continued to be grouped and modeled according to the above-described protocols (n ≥ 8), and 3 mice in each group were sacrificed to collect their lungs at 24 h and 48 h, respectively. The lungs were ground on ice and centrifuged to obtain a supernatant. Then, the supernatant was applied to an agar plate for determine the colony counts after incubation at 37 °C for 24 h. Meanwhile, the lungs and spleens of these mice sacrificed after 24 h in each group were obtained for H&E staining and pathological observation.

In vivo biosafety assessments

Finally, acute KPN-infected and TRKP-infected pneumonia mice were injected with saline (control group) and I-TPGS/Ga₂O₃/TIG (TIG: 15 mg/kg) to evaluate the *in vivo* biosafety of I-TPGS/Ga₂O₃/TIG (n=3). These mice were sacrificed at day 5, and their livers and kidneys were collected for H&E staining and pathological observation. Additionally, the mice were treated with saline (control group) and I-TPGS/Ga₂O₃/TIG nanoparticles (experimental group), then the whole blood of the mice was taken 5 days later. Blood analysis was performed to obtain relevant hematological parameters to further evaluate the biocompatibility of I-TPGS/Ga₂O₃/TIG nanoparticles.

Statistics

Each experiment was carried out in triplicate at least. Differences Comparative analysis between groups were analyzed with one-way analysis of variance (ANOVA) tests, and P-values < 0.05 were considered statistically significant. Values were presented as mean ± standard deviation (SD). All the

statistical analyses were performed on Graphic Pad 7.0 and Microsoft Excel software.

Abbreviations

TPGS: tocopherol polyethylene glycol succinate; KPN: *Klebsiella pneumoniae*; TRKP: tigecycline-resistant *Klebsiella pneumoniae*; TIG: tigecycline; Ga₂O₃: β-Ga₂O₃:Cr³⁺; I-TPGS/Ga₂O₃: anti-ICAM-TPGS/β-Ga₂O₃:Cr³⁺; DDS: nano-drug delivery system; ICAM1: intercellular Adhesion Molecule 1; TEM: transmission electron microscopy; XRD: X-ray powder diffraction; HUEVC: human umbilical endothelial vein cells; PSD: hydrodynamic particle size distribution; MIC: minimum inhibitory concentrations; MBC: minimum bactericidal concentrations; CFU: colony-forming unit; RT-PCR: reverse transcription polymerase chain reaction; H&E: haematoxylin-eosin.

Supplementary Material

Supplementary figures and table.

<http://www.thno.org/v09p2739s1.pdf>

Acknowledgements

This work was supported by the Scientific Research Fund of Ministry of Health - Medical Science Major Technology Fund Project of Zhejiang Province (WKJ-ZJ-1609) and New Century 151 Talent Project of Zhejiang Province.

Competing Interests

The authors have declared that no competing interest exists.

References

- Paczosa MK, Meccas J. *Klebsiella pneumoniae*: going on the offense with a strong defense. *Microbiol Mol Biol Rev.* 2016; 80: 629-61.
- Li B, Zhao Y, Liu C, Chen Z, Zhou D. Molecular pathogenesis of *Klebsiella pneumoniae*. *Future Microbiol.* 2014; 9: 1071-81.
- Lee C-R, Lee JH, Park KS, Jeon JH, Kim YB, Cha C-J, et al. Antimicrobial resistance of hypervirulent *Klebsiella pneumoniae*: epidemiology, hypervirulence-associated determinants, and resistance mechanisms. *Front Cell Infect Microbiol.* 2017; 7: 483.
- Daikos GL, Tsaousi S, Tzouveleki LS, Anyfantis I, Psychogiou M, Argyropoulou A, et al. Carbapenemase-producing *Klebsiella pneumoniae* bloodstream infections: lowering mortality by antibiotic combination schemes and the role of carbapenems. *Antimicrob Agents Chemother.* 2014; AAC. 02166-13.
- Wang X, Chen H, Zhang Y, Wang Q, Zhao C, Li H, et al. Genetic characterisation of clinical *Klebsiella pneumoniae* isolates with reduced susceptibility to tigecycline: role of the global regulator RamA and its local repressor RamR. *Int J Antimicrob Agents.* 2015; 45: 635-40.
- Jacobs DM, Safir MC, Huang D, Minhaj F, Parker A, Rao GG. Triple combination antibiotic therapy for carbapenemase-producing *Klebsiella pneumoniae*: a systematic review. *Ann Clin Microbiol Antimicrob.* 2017; 16: 76.
- Curcio D, Fernández F, Cané A, Barcelona L, Stamboulina D. Indications of a new antibiotic in clinical practice: results of the tigecycline initial use registry. *Braz J Infect Dis.* 2008; 12: 198-201.
- Li W, Huang L, Ying X, Jian Y, Hong Y, Hu F, et al. Corrigendum: Antitumor Drug Delivery Modulated by A Polymeric Micelle Having Upper Critical Solution Temperature. *Angew Chem Int Ed Engl.* 2015; 54: 6671.
- He Q, Shi J. MSN Anti-Cancer Nanomedicines: Chemotherapy Enhancement, Overcoming of Drug Resistance, and Metastasis Inhibition. *Adv Mater.* 2014; 26: 391-411.

10. Patel NR, Pattni BS, Abouzeid AH, Torchilin VP. Nanopreparations to overcome multidrug resistance in cancer. *Adv Drug Deliv Rev.* 2013; 65: 1748-62.
11. Nehme H, Saulnier P, Ramadan AA, Cassisa V, Guillet C, Eveillard M, et al. Antibacterial activity of antipsychotic agents, their association with lipid nanocapsules and its impact on the properties of the nanocarriers and on antibacterial activity. *PLoS One.* 2018; 13: e0189950.
12. Furneri PM, Fuochi V, Pignatello R. Lipid-based nanosized Delivery Systems for fluoroquinolones: A review. *Curr Pharm Des.* 2017; 23: 6696-704.
13. Almaaytah A, Mohammed GK, Abualhajaa A, Al-Balas Q. Development of novel ultrashort antimicrobial peptide nanoparticles with potent antimicrobial and antibiofilm activities against multidrug-resistant bacteria. *Drug Des Devel Ther.* 2017; 11: 3159.
14. Sharma S. Enhanced antibacterial efficacy of silver nanoparticles immobilized in a chitosan nanocarrier. *Int J Biol Macromol.* 2017; 104: 1740-5.
15. Liu G, Duan X, Li H, Liang D. Preparation and photoluminescence properties of Eu-doped Ga₂O₃ nanorods. *Mater Chem Phys.* 2008; 110: 206-11.
16. Nogales E, García JA, Méndez B, Piqueras J. Red luminescence of Cr in β-Ga₂O₃ nanowires. *J Appl Phys.* 2007; 101: 033517.
17. Wang X-S, Situ J-Q, Ying X-Y, Chen H, Pan H-f, Jin Y, et al. β-Ga₂O₃: Cr³⁺ nanoparticle: A new platform with near infrared photoluminescence for drug targeting delivery and bio-imaging simultaneously. *Acta Biomater.* 2015; 22: 164-72.
18. Assanhou AG, Li W, Zhang L, Xue L, Kong L, Sun H, et al. Reversal of multidrug resistance by co-delivery of paclitaxel and lonidamine using a TPGS and hyaluronic acid dual-functionalized liposome for cancer treatment. *Biomaterials.* 2015; 73: 284-95.
19. Wempe MF, Wright C, Little JL, Lightner JW, Large SE, Cafilisch GB, et al. Inhibiting efflux with novel non-ionic surfactants: Rational design based on vitamin E TPGS. *Int J Pharm.* 2009; 370: 93-102.
20. Roy S, Datta S, Viswanathan R, Singh AK, Basu S. Tigecycline susceptibility in *Klebsiella pneumoniae* and *Escherichia coli* causing neonatal septicemia (2007-10) and role of an efflux pump in tigecycline non-susceptibility. *J Antimicrob Chemother.* 2013; 68: 1036-42.
21. He F, Fu Y, Chen Q, Ruan Z, Hua X, Zhou H, et al. Tigecycline susceptibility and the role of efflux pumps in tigecycline resistance in KPC-producing *Klebsiella pneumoniae*. *PLoS One.* 2015; 10: e0119064.
22. De Majumdar S, Veleba M, Finn S, Fanning S, Schneiders T. Elucidating the Regulon of the Multi Drug Resistance Regulator RarA in *K. pneumoniae*. *Antimicrob Agents Chemother.* 2013; AAC. 01998-12.
23. Calderon AJ, Bhowmick T, Leferovich J, Burman B, Pichette B, Muzykantov V, et al. Optimizing endothelial targeting by modulating the antibody density and particle concentration of anti-ICAM coated carriers. *J Control Release.* 2011; 150: 37-44.
24. Garnacho C, Serrano D, Muro S. A fibrinogen-derived peptide provides intercellular adhesion molecule-1-specific targeting and intraendothelial transport of polymer nanocarriers in human cell cultures and mice. *J Pharmacol Exp Ther.* 2012; 340: 638-47.
25. Hsu J, Northrup L, Bhowmick T, Muro S. Enhanced delivery of α-glucosidase for Pompe disease by ICAM-1-targeted nanocarriers: comparative performance of a strategy for three distinct lysosomal storage disorders. *Nanomedicine.* 2012; 8: 731-9.
26. De Stoppelaar S, Van't Veer C, Roelofs J, Claushuis T, De Boer O, Tanck M, et al. Platelet and endothelial cell P-selectin are required for host defense against *Klebsiella pneumoniae*-induced pneumosepsis. *J Thromb Haemost.* 2015; 13: 1128-38.
27. Zhao W, Yang Y, Hao R, Liu F, Wang Y, Tan M, et al. Synthesis of mesoporous β-Ga₂O₃ nanorods using PEG as template: Preparation, characterization and photocatalytic properties. *J Hazard Mater.* 2011; 192: 1548-54.
28. Muruganandham M, Amutha R, Wahed MSA, Ahmad B, Kuroda Y, Suri RP, et al. Controlled fabrication of α-GaOOH and α-Ga₂O₃ self-assembly and its superior photocatalytic activity. *J Phys Chem C Nanomater Interfaces.* 2011; 116: 44-53.
29. Wang X-S, Li W-S, Situ J-Q, Ying X-Y, Chen H, Jin Y, et al. Multi-functional mesoporous β-Ga₂O₃: Cr³⁺ nanorod with long lasting near infrared luminescence for in vivo imaging and drug delivery. *RSC Adv.* 2015; 5: 12886-9.
30. Collnot E-M, Baldes C, Schaefer UF, Edgar KJ, Wempe MF, Lehr C-M. Vitamin E TPGS P-Glycoprotein Inhibition Mechanism: Influence on Conformational Flexibility, Intracellular ATP Levels, and Role of Time and Site of Access. *Mol Pharm.* 2010; 7: 642-51.
31. Vollmer W, Blanot D, De Pedro MA. Peptidoglycan structure and architecture. *FEMS Microbiol Rev.* 2008; 32: 149-67.
32. Zhao S, Tan S, Guo Y, Huang J, Chu M, Liu H, et al. pH-Sensitive Docetaxel-Loaded d-α-Tocopheryl Polyethylene Glycol Succinate-Poly(β-amino ester) Copolymer Nanoparticles for Overcoming Multidrug Resistance. *Biomacromolecules.* 2013; 14: 2636-46.
33. Ruzin A, Visalli MA, Keeney D, Bradford PA. Influence of transcriptional activator RamA on expression of multidrug efflux pump AcrAB and tigecycline susceptibility in *Klebsiella pneumoniae*. *Antimicrob Agents Chemother.* 2005; 49: 1017-22.
34. Smani Y, López-Rojas R, Domínguez-Herrera J, Docobo-Pérez F, Marti S, Vila J, et al. In vitro and in vivo reduced fitness and virulence in ciprofloxacin-resistant *Acinetobacter baumannii*. *Clin Microbiol Infect.* 2012; 18: E1-E4.
35. Smani Y, Domínguez-Herrera J, Pachón J. Association of the outer membrane protein Omp33 with fitness and virulence of *Acinetobacter baumannii*. *J Infect Dis.* 2013; 208: 1561-70.